Rapid Kinetic and Isotopic Studies on Dialkylglycine Decarboxylase†

Xianzhi Zhou,‡ Xueguang Jin, Rohit Medhekar, Xiangyang Chen,‡ Thorsten Dieckmann, and Michael D. Toney*

Department of Chemistry, University of California—Davis, One Shields Avenue, Davis, California 95161

Received May 31, 2000; Revised Manuscript Received August 24, 2000

ABSTRACT: The two half-reactions of the pyridoxal 5′-phosphate (PLP)-dependent enzyme dialkylglycine decarboxylase (DGD) were studied individually by multiwavelength stopped-flow spectroscopy. Biphasic behavior was found for the reactions of DGD-PLP, consistent with two coexisting conformations observed in steady-state kinetics [Zhou, X., and Toney, M. D. (1998) *Biochemistry 37*, 5761−5769]. The half-reaction kinetic parameters depend on alkali metal ion size in a manner similar to that observed for steady-state kinetic parameters. The fast phase maximal rate constant for the 2-aminoisobutyrate (AIB) decarboxylation half-reaction with the potassium form of DGD-PLP is 25 s^{-1}, while that for the transamination half-reaction between DGD-PMP and pyruvate is 75 s^{-1}. The maximal rate constant for the transamination half-reaction of the potassium form of DGD-PLP with L-alanine is 24 s^{-1}. The spectral data indicate that external aldimine formation with either AIB or L-alanine and DGD-PLP is a rapid equilibrium process, as is ketimine formation from DGD-PMP and pyruvate. Absorption ascribable to the quinonoid intermediate is not observed in the AIB decarboxylation half-reaction, but is observed in the dead-time of the stopped-flow in the L-alanine transamination half-reaction. The [1-^{13}C]AIB kinetic isotope effect (KIE) on k_{cat} for the steady-state reaction is 1.043 ± 0.003, while a value of 1.042 ± 0.009 was measured for the AIB half-reaction. The secondary KIE measured for the AIB decarboxylation half-reaction with [C4′-^{2}H]PLP is 0.92 ± 0.02. The primary [2-^{2}H]-L-alanine KIE on the transamination half-reaction is unity. Small but significant solvent KIEs are observed on k_{cat} and k_{cat}/K_M for both substrates, and the proton inventories are linear in each case. NMR measurements of C2−H washout vs product formation give ratios of 105 and 14 with L-alanine and isopropylamine as substrates, respectively. These results support a rate-limiting, concerted Cα-decarboxylation/C4′-protonation mechanism for the AIB decarboxylation reaction, and rapid equilibrium quinonoid formation followed by rate-limiting protonation to the ketimine intermediate for the L-alanine transamination half-reaction. Energy profiles for the two half-reactions are constructed.

Dialkylglycine decarboxylase (DGD)[1] is an intriguing PLP-dependent enzyme because it catalyzes both transamination and decarboxylation reactions in its normal catalytic cycle (Scheme 1). The enzyme was isolated from a soil bacterium (*1*) and transfers the fixed nitrogen from small 2,2-dialkylglycines, which are common in peptide antibiotics (*2*), onto pyruvate to give L-alanine. The decarboxylation half-reaction is highly specific for oxidative decarboxylation. Thus, the issue of reaction specificity has two main facets with this enzyme: control of decarboxylation vs transamination, and control of oxidative vs nonoxidative decarboxylation. The latter is addressed in this work.

Previous work has shown that DGD activity is dependent on alkali metal ions; potassium activates it while sodium inhibits it (*3*). The crystal structures of four different alkali metal liganded DGD forms have been reported (*4*−*6*). In solution, two coexisting, slowly interconverting conformations of homogeneously K^+-liganded DGD were demonstrated (*3*). These likely correspond to the K^+ and Na^+ forms observed in the crystal structures. The roles of several catalytically important pK_as, including one responsible for the interconversion of the two coexisting conformations, have been identified in an extensive pH study (*7*). Additionally, steady-state and pre-steady-state kinetic analyses of the DGD reactions with alternate substrates have shown that stereoelectronic effects play a role in determining decarboxylation vs transamination reactivity (*8*, *9*).

The first step of all PLP-dependent enzymes is formation of an external aldimine intermediate via a transimination reaction, displacing the active site lysine from its interaction with PLP (Scheme 1). In a classical stepwise decarboxylation mechanism, loss of the AIB α-carboxylate group as CO_2 from the external aldimine intermediate leads to the quinonoid intermediate, which, on protonation at C4′, gives the ketimine intermediate. These two steps could be concerted, as has been proposed for mechanistically different reactions

† Supported by Grant GM54779 to M.D.T. from the National Institutes of Health.

* To whom correspondence should be addressed. E-mail: toney@chem.ucdavis.edu. Phone: (530) 754-5282. Fax: (530) 752-8995.

‡ Current address: Monsanto Corporation, St. Louis, MO.

[1] Abbreviations: DGD, dialkylglycine decarboxylase; PLP, pyridoxal 5′-phosphate; PMP, pyridoxamine 5′-phosphate; DGD-PLP, PLP form of DGD; DGD-PMP, PMP form of DGD; DGD-K^+, DGD with potassium bound near the active site; DGD-Na^+, DGD with sodium bound near the active site; DGD-Rb^+, DGD with rubidium bound near the active site; AIB, 2-aminoisobutyrate; 2°ADH, NADP-dependent secondary alcohol dehydrogenase; AlaDH, L-alanine dehydrogenase; TEA, triethanolamine; bicine, *N*,*N*-bis[2-hydroxyethyl]glycine; SIE, solvent isotope effect; KIE, kinetic isotope effect.

10.1021/bi001237a CCC: $20.00
Published on Web 01/11/2001

Scheme 1

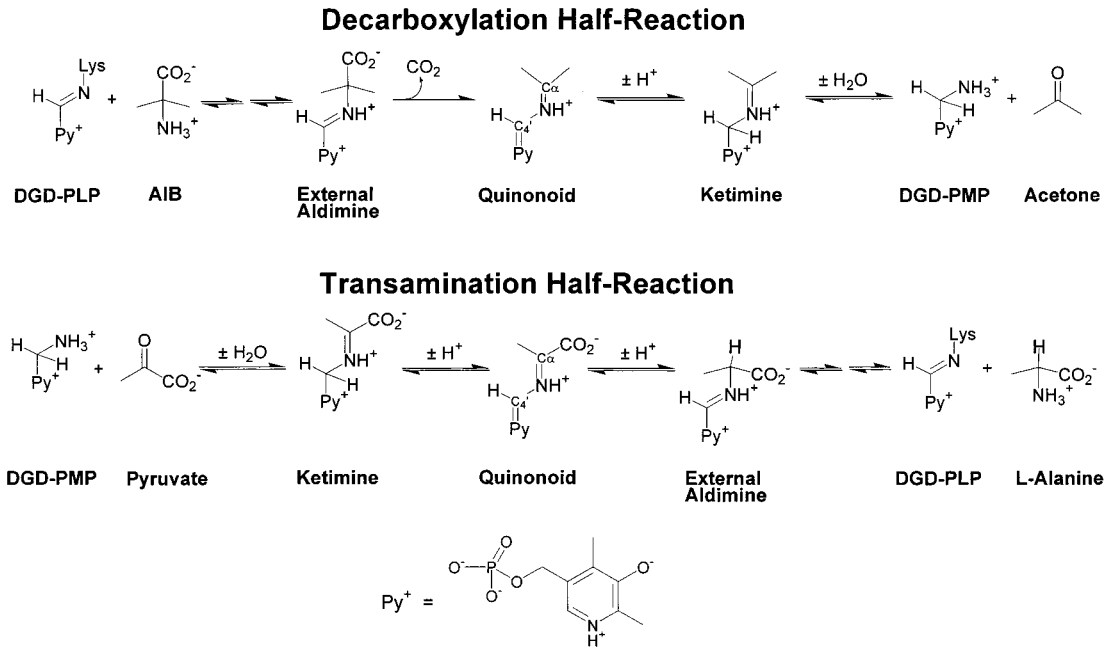

catalyzed by the PLP-dependent enzymes aspartate aminotransferase (*10*, *11*) and tryptophan indole-lyase (*12*). Regardless of whether decarboxylation is stepwise or concerted, the ketimine formed is hydrolyzed to produce DGD-PMP and acetone. This half-reaction is termed "oxidative decarboxylation" or "decarboxylation-dependent transamination" because the amino acid substrate is oxidized to a ketone instead of yielding an amine as in the reactions catalyzed by classical decarboxylases. The second half-reaction is a transamination between DGD-PMP and pyruvate. Proton abstraction from C4′ of the pyruvate ketimine gives a quinonoid intermediate, which leads to the L-alanine external aldimine via protonation on Cα. The final step of the catalytic cycle is transimination to release L-alanine as the amino acid product.

Here, a series of stopped-flow, kinetic isotope effect, and NMR experiments are described. These studies show that the decarboxylation half-reaction is largely rate-determining for the catalytic cycle and that formation of aldimines and ketimines with all substrates is rapid. For the AIB decarboxylation half-reaction, the lack of a detectable quinonoid intermediate, a large [^{13}C]KIE on decarboxylation, a significant solvent KIE originating from a single proton, a large inverse secondary [^{2}H]KIE on decarboxylation with [^{2}H]PLP, and a greater than unity washout to product formation ratio with isopropylamine all combine to support a concerted decarboxylation/proton-transfer mechanism. For the L-alanine/pyruvate transamination half-reaction, the observation of a quinonoid intermediate in the dead-time of the stopped-flow, the lack of a primary KIE with [^{2}H]alanine, and the large washout to product formation ratio combine to support a mechanism in which, surprisingly, protonation of the quinonoid intermediate is rate determining.

EXPERIMENTAL PROCEDURES

Materials. AIB, pyruvic acid, L-alanine, β-hydroxypyruvate, PLP, NADPH, 2°ADH were purchased from Sigma. Succinic acid, potassium hydroxide, bicine, sodium borodeuteride (99% D), manganese dioxide, and phenetidine hydrochloride were from Aldrich. [2-^{2}H]-L-Alanine (99% D) and deuterium oxide (99.9% D) were from Cambridge Isotope Laboratories. PMP was synthesized as described (*3*).

Synthesis of [4′-^{2}H]Pyridoxal 5′-Phosphate. Pyridoxal 5′-phosphate (1 g, 4 mmol) was reduced by one-half equivalent of sodium borodeuteride at neutral pH in 25 mL of water. The pH was lowered to 3 and the reaction mixture was rotary evaporated three times from methanol to remove borate. The pH of the reaction mixture was brought to 1 and excess manganese dioxide (7−8 equiv) was added. The oxidation reaction was stirred overnight under nitrogen at room temperature. Manganese dioxide was removed by filtration through Celite, and the pH of the filtrate was raised to 7 with KOH. The yield of crude [2-^{2}H]PLP was ∼50% as determined spectrophotometrically. The phenetidine Schiff base of PLP was isolated (*13*). It was hydrolyzed by dissolution in 5 mL of concentrated HCl and purified on the H^+ form of Bio-Rex 70 (Bio-Rad) with 1 M HCl as the eluting solvent. The overall yield was ∼20%. The purified [4′-^{2}H]pyridoxal-5′-phosphate showed the expected ^{1}H NMR spectrum (*14*) with ∼5% aldehyde remaining.

Synthesis of [1-^{13}C]AIB. The Strecker synthesis with labeled cyanide was employed. To a sealed tube containing 1.7 g of NH_4Cl, 2.2 mL of concentrated NH_4OH, and 2.0 g of $K^{13}CN$ in 7.6 mL of water, 2.4 mL of acetone in 9.6 mL of ethanol was added dropwise while stirring. The tube was sealed and heated at 70 °C overnight. The resulting solution was cooled to 0 °C, poured into 34 mL of ice-cold concentrated HCl, and saturated with dry HCl gas. After standing in ice for 5 h, the mixture was refluxed for 3 h. The solvent was evaporated and then coevaporated with a mixture of ethanol-toluene. The residue was suspended in 100 mL of anhydrous ethanol and refluxed for 1 h. The resulting ethanol-insoluble solid was filtered and refluxed with another 100 mL of anhydrous ethanol for an additional hour. After filtration, the two filtrates were combined, concentrated, and neutralized with 10 mL of concentrated

NH_4OH, and evaporated to dryness. The crude product was dissolved in about 1 mL of deionized water and loaded onto a 2 × 30 cm Amberlite IR-120 ion-exchange column. The column was washed with deionized water, and the product eluted with 2 M NH_4OH. The desired [1-^{13}C]AIB product was further purified by recrystallization from water-ethanol with a final yield of ~50% based on the starting K^{13}CN. ^{1}H NMR (300 MHz, D_2O) δ 1.60 (d, J = 3.8 Hz); ^{13}C NMR (75 MHz, D_2O) δ 23.9, 58.6 (d, J = 54 Hz), 178.3.

[1-^{13}C]AIB Steady-State Kinetic Isotope Effect. The steady-state KIE on k_{cat} was measured using the continuous-flow apparatus described previously (*15*). The conditions were 40 mM bicine-KOH, pH 8.0, 50 mM dipotassium succinate, 5 mM disodium succinate, 25 mM [1-^{13}C]AIB or unlabeled AIB, 3 units/mL 2°ADH, 300 μM NADPH, 20 μM PLP, and 25 °C.

Stopped-Flow Kinetic Studies of the Decarboxylation Half-Reaction. An Applied Photophysics SX.17MV stopped-flow spectrophotometer was used. Both DGD-PLP and AIB were in 30 mM bicine-KOH, pH 8.2, 100 mM dipotassium succinate. DGD-PLP (final concentration, 13 μM) was rapidly mixed with an equal volume of AIB of various concentrations ranging from 0.05 to 40 mM. In some experiments, single wavelength kinetic traces were collected with a photomultiplier and monochromator. Generally, absorbance scans from 300 to 550 nm were collected on a logarithmic time scale with a UV-enhanced diode-array detector (2.56 ms scan time) at 25 °C. The spectra were analyzed globally using SPECFIT (Spectrum Software Associates).

DGD-Rb^+ was prepared by dialysis of DGD-K^+ against 30 mM bicine-RbOH, pH 8.2, 100 mM dirubidium succinate. The reactions of the PLP form of DGD-Rb^+ with AIB were conducted as described above for DGD-K^+, with Rb^+ replacing K^+.

The half-reaction kinetic isotope effects measured with [1-^{13}C]AIB and [C4′-^{2}H]PLP were measured under identical reaction conditions. A Bio-Logic SFM-400 stopped-flow mixer and a J&M Tidas diode-array detector were employed. Spectra (256) were collected over 4 s and analyzed with SPECFIT to obtain rate constants and spectra for intermediates. The [1-^{13}C]AIB KIE was measured by directly comparing the rate constants for AIB and [1-^{13}C]AIB. The reaction conditions were 40 mM bicine-KOH, pH 8.2, 50 mM dipotassium succinate, 5 mM disodium succinate, 100 μM PLP. The final concentrations of DGD-PLP and AIB were ~10 μM and 20 mM, respectively.

For the [C4′-^{2}H]PLP KIEs, apoDGD was prepared by overnight dialysis at 4 °C against two changes of 40 mM bicine-KOH, 50 mM dipotassium succinate, and 5 mM disodium succinate, pH 8.2. ApoDGD was divided into two parts and 100 μM PLP or [C4′-^{2}H]PLP added and allowed to bind for 1 h on ice. Reactions were initiated by mixing equal volumes of DGD-PLP and AIB, each in 40 mM bicine-KOH, 50 mM dipotassium succinate, and 5 mM disodium succinate, pH 8.2. The final concentrations of DGD-PLP and AIB were 24 μM and 20 mM, respectively.

Stopped-Flow Kinetic Studies of the DGD-PMP Transamination Half-Reaction with Pyruvate. DGD-PMP prepared in two ways was compared because of the relatively fast dissociation of PMP from DGD (half-life = ~15 min at pH 8 and 25 °C). In the first method, DGD-PMP was prepared in situ by reaction of limiting AIB with excess DGD-PLP and immediately mixed with various concentrations of pyruvate in the stopped-flow. Multiple single wavelength absorbance traces from 300 to 550 nm (logarithmic time scale; 10 nm interval) were collected using the SX.17MV stopped-flow since the half-life of the fast phase is short compared to the sampling time of the diode-array detector. In the second method, apoDGD was prepared as described above and incubated with a saturating concentration of PMP (6 mM) and 100 mM KCl. This DGD-PMP was mixed with pyruvate, and multiple single wavelength traces from only 370 to 550 nm were taken, due to the high absorbance of free PMP. Traces were fitted both globally and individually using Pro-Kineticist software supplied by Applied Photophysics. The reaction conditions were identical to those for the DGD-PLP reactions.

Stopped-Flow Kinetic Studies of the DGD-PLP Transamination Half-Reaction with L-Alanine. Transamination reactions of DGD-PLP with both L-alanine and [2-^{2}H]-L-alanine were followed as described above for AIB using the SX.17MV stopped-flow. The concentrations of L-alanine and [2-^{2}H]-L-alanine were accurately measured using L-alanine dehydrogenase in 50 mM borate-KOH, pH 10.0, 5 mM NAD^+, 4 units/mL AlaDH, and 100 mM KCl. For the solvent isotope effects on these reactions, buffer and reagents were prepared directly in D_2O. The small amount of protium introduced was ignored.

The PLP form of DGD-Rb^+ was reacted with L-alanine as described above for AIB. Additionally, reactions were performed after incubation for 30 min with 15 mM aminocyclopropane carboxylate, a competitive inhibitor of DGD. The reactions were performed at a single L-alanine concentration of 40 mM, with a final concentration of 1.5 mM aminocyclopropane carboxylate.

Steady-State Kinetics. Solvent isotope effects were measured by coupling the acetone produced from the AIB/pyruvate reaction to 2°ADH and monitoring the decrease in NADPH absorbance at 340 nm using a Kontron Uvikon 9420 spectrophotometer. The reaction conditions were 30 mM bicine-KOH, pH 8.2, 50 mM dipotassium succinate, 0.5 unit/mL 2°ADH, 0.2 mM NADPH. Two stocks of reagents were prepared, one in H_2O, and one in D_2O. These were mixed to give the appropriate atom fraction D_2O in proton inventory experiments. For SIEs on k_{cat}, saturation curves were measured using a substrate mixture of AIB and pyruvate in which the ratio of their concentrations was equal to the ratio of their K_m values. For SIEs on k_{cat}/K_{AIB}, pyruvate was fixed at 1 mM, and AIB saturation curves were measured in various atom fractions of D_2O. For SIEs on k_{cat}/K_{pyr}, the AIB concentration was fixed at 2 mM, and saturation curves for pyruvate were measured.

The heat of activation for k_{cat} and k_{cat}/K_{AIB} was measured in 0.1 M potassium phosphate buffer, pH 7.8, using the 2°ADH coupled assay in the temperature range of 10−40 °C.

NMR Determination of Washout vs Product Formation Ratios. For the transamination reactions of L-alanine and isopropylamine, the peaks for the C2 hydrogens of the substrates and for the methyl groups of the ketone products were followed by NMR at 25 °C. The integrated intensities (normalized by the number of hydrogens contributing to each

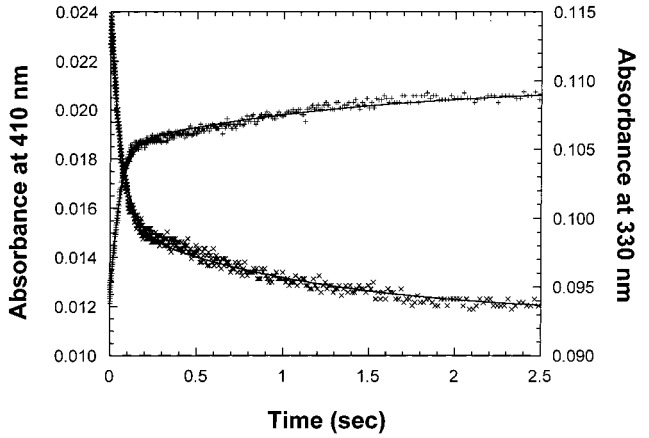

FIGURE 1: Absorbance traces for the decarboxylation half-reaction of DGD-PLP with AIB. The traces at both 410 and 330 nm show clear biphasicity, due to coexisting fast and slow reacting enzyme conformations in the potassium form of the enzyme. Experimental conditions: 13 μM DGD-PLP, 40 mM AIB, 30 mM bicine-KOH, pH 8.2, 100 mM dipotassium succinate, 25 °C.

peak) vs time were plotted to obtain the relative rates of C2−H washout vs product formation.

A 300 MHz Bruker spectrometer was employed for the characterization of alanine transamination products. Reactions contained 100 mM potassium phosphate, pH 7.8, 50 mM L-alanine, 5 mM β-hydroxypyruvate, 100 μM PLP, 0.4 μM DGD, and 0.2 mM TSP in D_2O. The reaction was initiated with enzyme and spectra were collected at ~2 min intervals over 1 h. Due to the very low transamination reactivity of isopropylamine, this reaction was measured using a 600 MHz Bruker DRX spectrometer. Mild solvent presaturation was used. One spectrum consisted of 128 scans with a relaxation delay of 2.5 s. Reactions contained 100 mM potassium phosphate, pH 7.8, 25 mM isopropylamine, 10 mM β-hydroxypyruvate, 200 μM PLP, 4 μM DGD, and 0.2 mM TSP in D_2O. Reactions were initiated with enzyme and spectra were collected at 9 min intervals over 4 h.

RESULTS

Heats of Activation. The heats of activation for k_{cat} and k_{cat}/K_{AIB} were found to be 9.8 ± 0.7 and 12.7 ± 0.9 kcal/mol, respectively, using AIB and pyruvate as substrates.

DGD-PLP Decarboxylation Half-Reaction with AIB. Absorbance data at the spectral maxima (410 and 330 nm) clearly show the biphasic behavior of the potassium form of DGD-PLP (Figure 1). Multiwavelength data show a decrease in the absorbance at 410 nm, concomitant with an increase in absorbance at 330 nm and a shift in the λ_{max} of the remaining aldehydic absorbance to 395 nm. Global analysis of the multiwavelength data using a two-step, serial mechanism (eq 1) in SPECFIT gives spectra for three species (A, B, and C; Figure 2A)

$$A \xrightarrow{k_1} B \xrightarrow{k_1} C \qquad (1)$$

An isosbestic point at 352 nm is observed with no absorbance at ~500 nm, characteristic of a quinonoid intermediate (*16*). The observed rate constants from the global fits increase hyperbolically with AIB concentration, with apparent *y*-intercepts of zero. An *F*-test showed that the fit to a rectangular hyperbola with an offset is not significantly better than that without an offset. The kinetic parameters obtained are given in Table 1. The maximal fast phase rate constant is 24.5 ± 0.3 s^{-1} with K_{app} = 2.0 ± 0.1 mM, while the maximal slow phase rate constant is 0.73 ± 0.02 s^{-1} with K_{app} = 0.47 ± 0.06 mM.

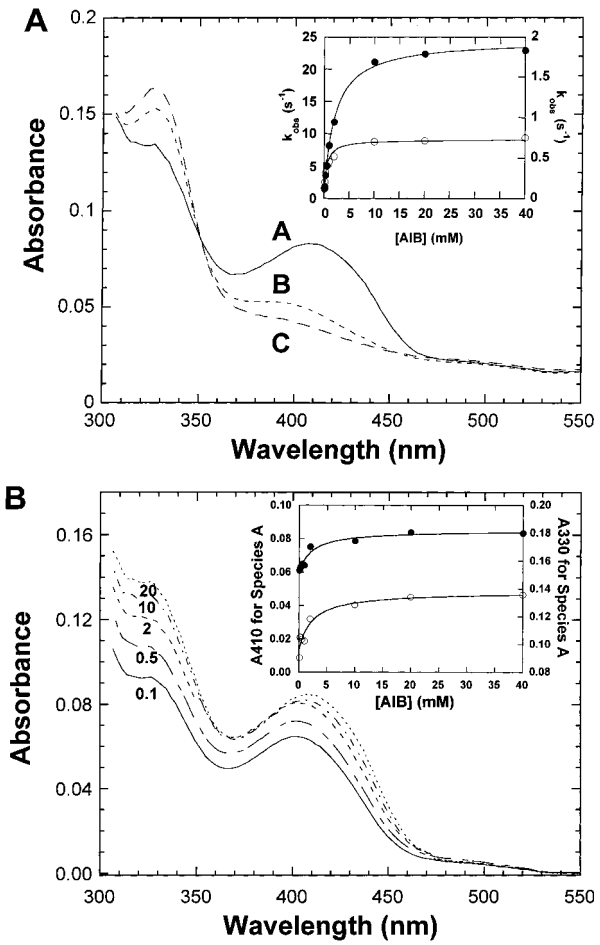

FIGURE 2: (A) Absorbance spectra for the three species in a serial, two-step mechanism obtained from the analysis of multiwavelength data collected in the DGD-PLP half-reaction with AIB. The inset shows the concentration dependence of the pseudo-first-order rate constants (fast phase, closed circles; slow phase, open circles). Experimental conditions as in Figure 1. (B) Spectra of species A from global analysis as a function of AIB concentration. The concentrations are indicated on the spectra. The inset shows the concentration dependence of the 410 (open circles) and 330 nm absorbance (closed circles).

Figure 2b shows the spectra of species A, obtained from the global analyses of the multiwavelength data, as a function of AIB concentration. The absorbance at 410 and 330 nm on species A increases hyperbolically with AIB concentration (inset Figure 2b); fitting to a rectangular hyperbola with an offset gives K_{app} = 2.2 ± 0.5 and 2 ± 1 mM for the 410 and 330 nm data, respectively. These are identical, within error, to that obtained from the fast phase rate constants (Table 1).

DGD-PLP Transamination Half-Reaction with L-Alanine. The transamination half-reaction with L-alanine is also a biphasic process and shows absorbance changes at 410 and 330 nm similar to those observed in the AIB decarboxylation half-reaction. In contrast to the AIB reaction, clear absorbance at 495 nm is observed in the first spectrum collected

Table 1: Half-Reaction Kinetic Parameters[a]

	fast phase		slow phase		fast phase amplitude (%)	quinonoid observed
	k_{max}^{fast} (s^{-1})	K_{app}^{fast} (mM)	k_{max}^{slow} (s^{-1})	K_{app}^{slow} (mM)		
potassium form of DGD						
DGD-PLP + AIB	24.5 (0.3)	2.0 (0.1)	0.73 (0.02)	0.47 (0.06)	69	no
DGD-PLP + AIB + ACPC	13.6 (0.1)		1.3 (0.2)		17	no
DGD-PLP + L-alanine	23.6 (0.7)	6.6 (0.7)	1.25 (0.05)	2.6 (0.4)	70	yes
DGD-PMP + pyruvate	75 (2)	1.1 (0.1)				yes
rubidium form of DGD						
DGD-PLP + AIB	16.7 (0.2)	3.5 (0.2)	3.1 (0.3)	1.1 (0.4)	61	no
DGD-PLP + L-alanine	24 (1)	21 (2)	2.3 (0.5)	3.7 (0.3)	65	yes
sodium form of DGD						
DGD-PLP + AIB			1.5 (0.1)		~0	no

[a] Standard errors are given in parentheses. Reaction conditions: 30 mM bicine-alkali metal hydroxide, pH 8.2, 100 mM alkali metal salt of succinate, ~12 μM DGD subunits, 50 μM PLP and varying concentrations of substrate. DGD-PMP was prepared by either reaction with substoichiometric concentrations of AIB or reconstitution of apoenzyme with excess PMP. PMP was present at a final concentration of 2 mM in the latter reactions. The reaction with ACPC preincubation (15 mM) was performed at a single, saturating concentration (100 mM) of AIB, as was the reaction of the sodium form of DGD. The amplitudes were calculated from absorbance values at 430 and 330 nm.

by the diode-array detector. Figure 3 presents results obtained with L-alanine. The maximal rate constants for the alanine transamination half-reaction are 23.6 ± 0.7 and 1.25 ± 0.05 s^{-1}, while K_{app} values are 6.6 ± 0.7 and 2.6 ± 0.4 mM for the fast and slow forms, respectively. An *F*-test showed that the fit to a rectangular hyperbola with an offset is not significantly better than that without an offset.

Global analysis of the multiwavelength data provides the spectra for the three species in the biphasic process. The spectra of species A have clear absorbance at 495 nm, which is characteristic of a quinonoid intermediate (*16*). Also, the spectra of species A show a hyperbolic dependence on alanine concentration, similar to that observed with AIB. The 330 and 410 nm data in the spectra of the first species both give $K_{app} = 7 \pm 2$ mM. The 495 nm data, on the other hand, give $K_{app} = 40 \pm 19$ mM.

DGD-PMP Transamination Half-Reaction with Pyruvate. DGD-PMP prepared in situ with AIB and from apoDGD behaved similarly. Since this half-reaction is relatively fast, kinetic traces at 10 nm intervals were individually collected using a photomultiplier, and multiwavelength spectra were reconstructed from these. The 330 nm absorbance decreased and that at 410 nm increased in an apparent single-exponential process in the time range of 10−100 ms. The spectra obtained from global analysis of this time range are presented in Figure 4A. The maximal rate constant for this reaction is 75 ± 2 s^{-1}, while $K_{app} = 1.1 \pm 0.1$ mM (Figure 4A, inset, and Table 1). The concentration dependence of the 320 nm absorbance of species (Figure 4B) gives $K_{app} = 0.8 \pm 0.4$ mM.

The absorbance at 495 nm, on the other hand, increased rapidly to a maximum at ~6 ms and then decayed, as seen in Figure 5. The fitted lines shown are simple two exponential fits. The rate constants obtained from these are plotted against pyruvate concentration in the Figure 5, inset. The slow phase shows pyruvate dependence with a maximal rate constant of 80 ± 8 s^{-1} and $K_{app} = 1.4 \pm 0.6$ mM. The fast phase is apparently independent of pyruvate concentration at a value of 286 ± 20 s^{-1}. Global fitting of these concentration dependent data (using KINSIM/FITSIM) to a preassociation mechanism, eq 2, with $K_d = 1.1$ mM gave a similar value

$$A + B \overset{K_d}{\rightleftharpoons} C \xrightarrow{k_1} D \xrightarrow{k_2} E \qquad (2)$$

Table 2: Steady-State Kinetic Isotope Effects[a]

	k_{cat}	k_{cat}/K_{AIB}	k_{cat}/K_{pyr}
D_2O	1.54 (0.03) [1.61 (0.01)][b]	1.47 (0.02)	1.85 (0.02)
proton inventory	linear	linear	linear
[1-^{13}C]-AIB	1.043 (0.003)		

[a] Standard errors are given in parentheses. Reaction conditions: 30 mM bicine-KOH, pH 8.2, 50 mM dipotassium succinate, 5 mM disodium succinate, 50 μM PLP. [b] Taken from ref *15*, in which this value was measured in a proton inventory experiment.

of the slow rate constant but a fast phase rate constant that is highly correlated with the value of the extinction coefficient assumed for the quinonoid intermediate. Previous work suggests a value of ~35 000 M^{-1} cm^{-1} (*16*), which yields values of >500 s^{-1} for the fast phase rate constant.

Kinetic Isotope Effects. The proton inventories on k_{cat} measured here and previously (*15*) are both linear. Similar KIEs of 1.54 ± 0.03 and 1.61 ± 0.01 were obtained from these separate experiments (Table 2). The proton inventories on k_{cat}/K_{AIB} and k_{cat}/K_{Pyr} are similarly linear. These are shown in Figure 6. The KIEs obtained for these parameters are 1.47 ± 0.02 and 1.85 ± 0.02 (Table 2).

The [1-^{13}C]AIB steady-state KIE on k_{cat} was measured to be 1.043 ± 0.003 using the continuous-flow method. The same KIE was measured for the AIB decarboxylation half-reaction with saturating AIB using the stopped-flow, and was found to be 1.042 ± 0.009 (Table 3). The [4′-^{2}H]PLP KIE was found to be inverse with a value of 0.92 ± 0.02 for the AIB decarboxylation half-reaction with saturating AIB using the stopped-flow.

The L-alanine half-reaction was probed isotopically using saturating concentrations of substrate (Table 3). The [2-^{2}H]-L-alanine KIE on the fast phase is unity within error in both H_2O and D_2O, while the solvent KIE is ~1.5 with either labeled or unlabeled L-alanine. The [2-^{2}H]-L-alanine KIE on the slow phase is significant, as is the D_2O effect. The data suggest an apparent decrease in each KIE when combined with the other isotopically labeled species, although the errors preclude definitive conclusions.

NMR Determination of Washout vs Product Formation Ratios. The reactions of DGD-PLP with both L-alanine and isopropylamine were followed by ^{1}H NMR (Figure 7). The

Table 3: Half-Reaction Kinetic Isotope Effects[a]

isotopically labeled reactant	KIE on k_{fast}	KIE on k_{slow}
AIB reactions		
[1-^{13}C]-AIB[b]	1.042 (0.009)	
[4-^{2}H]-PLP[b]	0.92 (0.02)	
L-alanine reactions		
D_2O with [2-^{1}H]-L-Ala[b]	1.6 (0.1)	2.1 (0.2)
D_2O with [2-^{2}H]-L-Ala[b]	1.5 (0.1)	2.0 (0.1)
[2-^{2}H]-L-Ala with H_2O[c]	1.02 (0.02)	1.30 (0.09)
[2-^{2}H]-L-Ala with D_2O[c]	1.05 (0.09)	1.24 (0.08)

[a] Standard errors are given in parentheses. Values are averages of at least three measurements. [b] Reaction conditions: 30 mM bicine-KOH, pH 8.2, 13 μM DGD, 20 mM AIB, or 60 mM L-alanine, 50 mM dipotassium succinate, 5 mM disodium succinate, 50 μM PLP. The concentrations of AIB were determined by copper complexation. The concentrations of alanine were determined using alanine dehydrogenase. [c] Reaction conditions: 30 mM bicine-KOH pH 8.2, 13.2 μM DGD, 50 mM dipotassium succinate, 5 mM disodium succinate, 50 μM PLP. Saturation curves for both L-alanine and [2-^{2}H]-L-alanine were measured.

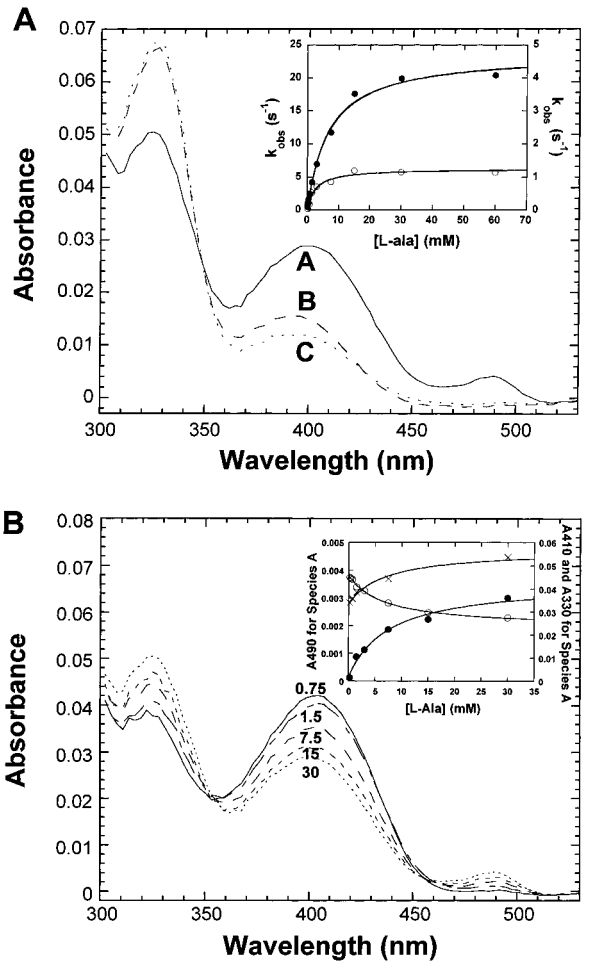

FIGURE 3: (A) Absorbance spectra for the three species in a serial, two step mechanism obtained from the analysis of multiwavelength data collected in the DGD-PLP half-reaction with L-alanine. The inset shows the concentration dependence of the pseudo-first-order rate constants (fast phase, closed circles; slow phase, open circles). Experimental conditions: 13 μM DGD-PLP, 30 mM L-alanine, 30 mM bicine-KOH, pH 8.2, 100 mM dipotassium succinate, 25 °C. (B) Spectra of species A from global analysis as a function of L-alanine concentration. The concentrations are indicated on the spectra. The inset shows the concentration dependence of the 410 (open circles) and 330 nm (crosses) absorbance, as well as that for 490 nm (closed circles).

loss of the signal from the C2−H and product formation were followed simultaneously. Loss of the C2−H signal arises from both washout and product formation. The rate of washout was thus calculated by subtracting the rate of product formation from the rate of loss of the C2−H signal. The isomerization of the fast to slow enzyme form was evident in the L-alanine reactions, and the data were thus fitted to eq 3, which describes a hysteretic enzyme.

$$[P] = v_{ss}t - \frac{(v_{ss} - v_i)(1 - e^{-kt})}{k} \quad (3)$$

The ratio of washout to product formation was found to be 105 ± 30 for L-alanine and 14 ± 1 for isopropylamine.

DISCUSSION

Coexisting Enzyme Forms. Previous work (*3*) demonstrated that the potassium form of DGD-PLP exists in solution as a mixture of two kinetically distinguishable forms. The slower reacting form has a lower K_{AIB}, and a substrate concentration dependent transition of the faster to the slower form is observed in initial rate measurements over ~15 min. DGD has two alkali metal ion binding sites per monomer, one of which is near the active site and will accept a variety of alkali metal ions (*4*−*6*). The multiple enzyme forms in solution are consistent with the structural transition observed as a function of alkali metal ion size; the larger Rb^+ and K^+ ions are activators and share the same protein structure, whereas the smaller Na^+ and Li^+ ions are inhibitors and share a protein structure different from that of the larger ions.

The data in Table 1 and Figure 1 corroborate, through analysis of the individual half-reactions, that the potassium and rubidium forms of DGD-PLP exist as a mixture of slow and fast reacting enzyme forms. As predicted from the transition from fast to slow enzyme in initial rate measurements, the slow form has a lower K_{AIB}. The experiment in which DGD-PLP was preincubated with 1-aminocyclopropane carboxylate, a competitive inhibitor of DGD-PLP, confirms the steady-state observation that preincubation with this inhibitor draws the equilibrium between the two forms toward the tighter binding, slower reacting form. Here, the amplitude of the fast phase of the AIB half-reaction is reduced from 69 to 17% by preincubation with inhibitor.

Analysis of the half-reactions of both the potassium and rubidium forms of DGD-PLP with AIB and L-alanine demonstrates the presence of fast and slow reacting forms in each case. The half-reaction kinetic parameters vary substantially between the potassium and rubidium forms, with the slow form retaining its higher apparent affinity for substrates compared to the fast form.

On the other hand, the reaction of the sodium form of DGD-PLP shows no clear indication of a fast-reacting enzyme form, although a few percent of fast-reacting enzyme might not be detectable in the stopped-flow traces. Thus, the structural, steady-state, and half-reaction kinetic data form a self-consistent model in which the larger alkali metal ions activate the enzyme by driving the conformational equilibrium largely but not fully toward the fast reacting conformation, while the smaller alkali metal ions promote nearly complete formation of the slow reacting conformation.

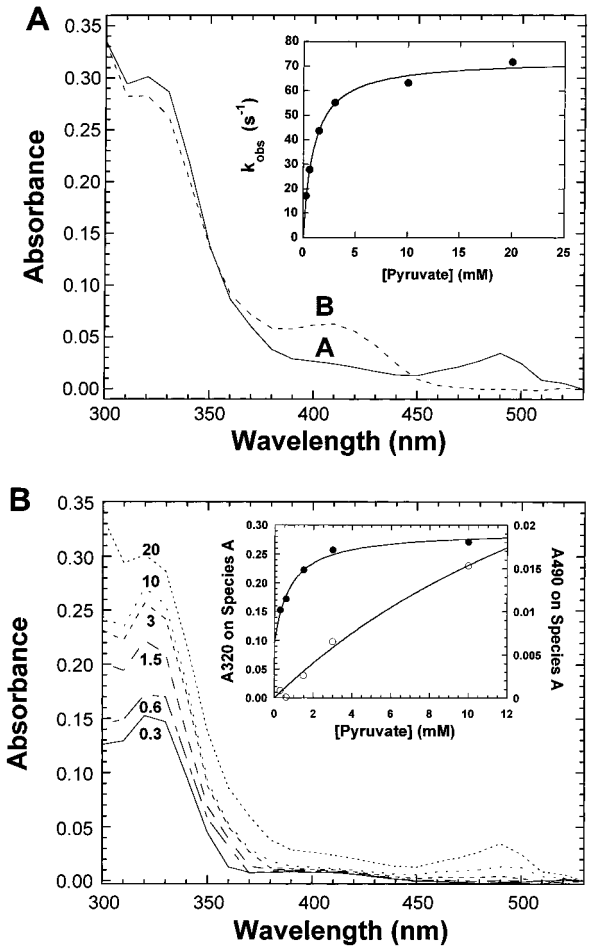

FIGURE 4: (A) Absorbance spectra from global analysis of the DGD-PMP half-reaction with pyruvate using a single-exponential model. Data between 10 and 100 ms were analyzed. The inset shows the concentration dependence of the pseudo-first-order rate constants. Experimental conditions: 13 μM DGD-PLP, 20 mM pyruvate, 30 mM bicine-KOH, pH 8.2, 100 mM dipotassium succinate, 25 °C. (B) The spectra of species A from global analysis as a function of pyruvate concentration. The concentrations are indicated on the spectra. The inset shows the concentration dependence of the 320 (closed circles) and 490 nm (open circles) data.

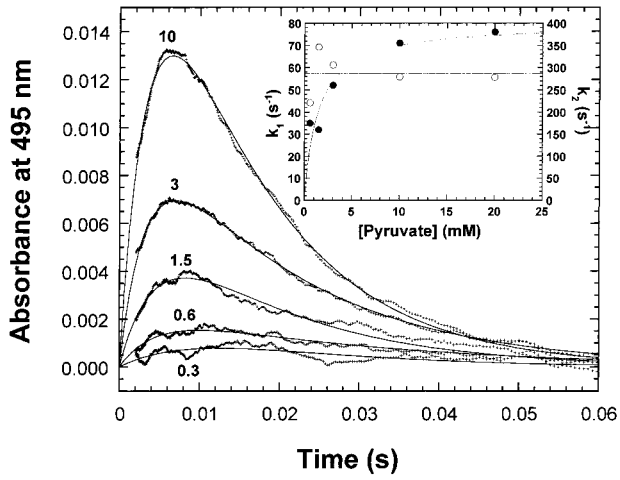

FIGURE 5: Absorbance traces at 490 nm for the DGD-PMP half-reaction with pyruvate. The concentrations of pyruvate are indicated. The traces were fitted to a simple two exponential model, shown as the solid lines. The inset shows the concentration dependence of the observed rate constants for the fast (open circles) and slow (closed circles) phases. Reaction conditions as in Figure 4.

Unlike DGD-PLP, the apparent absence of a slow reacting enzyme form in the DGD-PMP reaction with pyruvate suggests that this enzyme form exists as a single conformer.

Rapid Equilibrium Aldimine and Ketimine Formation. Previous experiments, in which the half-reaction of the potassium form of DGD-PLP with L-alanine was fully coupled kinetically to the lactate dehydrogenase catalyzed reduction of pyruvate with NADH, demonstrated that ketimine hydrolysis and dissociation of pyruvate from DGD-PMP is rapid (*3*). The pH dependence of the steady-state kinetic parameters and inhibition constants (*7*) demonstrated that AIB binding to the potassium form of DGD-PLP is also a rapid equilibrium process. These previous results are corroborated by the experiments reported here.

Global analysis of the multiwavelength data sets for the half-reactions provides both rate constants and true spectra of the kinetically significant species. The spectrum of the first species is the spectrum of the reactant/product mixture after ~1.5 ms of reaction (the dead-time of the stopped-flow). The previous results cited above indicate that this species should, in all cases here, be the spectrum of the enzyme rapidly equilibrated with substrate.

The K_{app} values obtained from the concentration dependence of the spectra of the first species agree with those obtained from the concentration dependence of the observed rate constants. The respective values obtained from rate constants and spectra, respectively, are AIB, 2.0 vs 2.2 and 2 (410 and 330 nm, respectively); L-alanine, 6.6 vs 7; and pyruvate, 1.1 vs 0.8. This provides strong independent evidence for these substrates that binding and aldimine or ketimine formation is at equilibrium within the 1.5 ms dead-time of the stopped-flow. Given this, lower limits for these bimolecular rate constants of $\sim 3 \times 10^5$ M^{-1} s^{-1} can be estimated. This is well above the steady-state k_{cat}/K_{AIB} value of ~7000 M^{-1} s^{-1} and the k_{cat}/K_{pyr} value of $\sim 1 \times 10^5$ M^{-1} s^{-1}.

Transamination Quinonoid Intermediate. Table 1 and Figures 2−5 show that the quinonoid intermediate is consistently observed in the L-alanine/pyruvate transamination half-reaction for the various metal ion forms, but not in the AIB decarboxylation half-reaction. Quinonoid absorbance at 495 nm in the L-alanine transamination half-reaction is at initial equilibrium within the 1.5 ms dead-time of the stopped-flow. Thus, *within 1.5 ms*, L-alanine reacts with DGD-PLP to equilibrate through the reaction sequence of Michaelis complex formation, transimination to the external aldimine intermediate, and deprotonation to the quinonoid intermediate (Scheme 1). This suggests that the rate-limiting step in the L-alanine transamination half-reaction is quinonoid protonation at C4′ to give the ketimine intermediate.

The KIEs measured for the L-alanine half-reaction support the conclusion that quinonoid protonation at C4′ is the rate-limiting step in transamination. The primary KIE has a value of ~1 in both H_2O and D_2O, while the solvent KIEs are ~1.5. This indicates that the Cα proton is not in flight in the rate-limiting step, but that a solvent derived proton is. It is tempting to assign this solvent proton to one on Lys272, the general acid/base catalyst in transamination, but others are possible. For example, proton transfers to or from either the pyridine or the aldimine nitrogens are candidates.

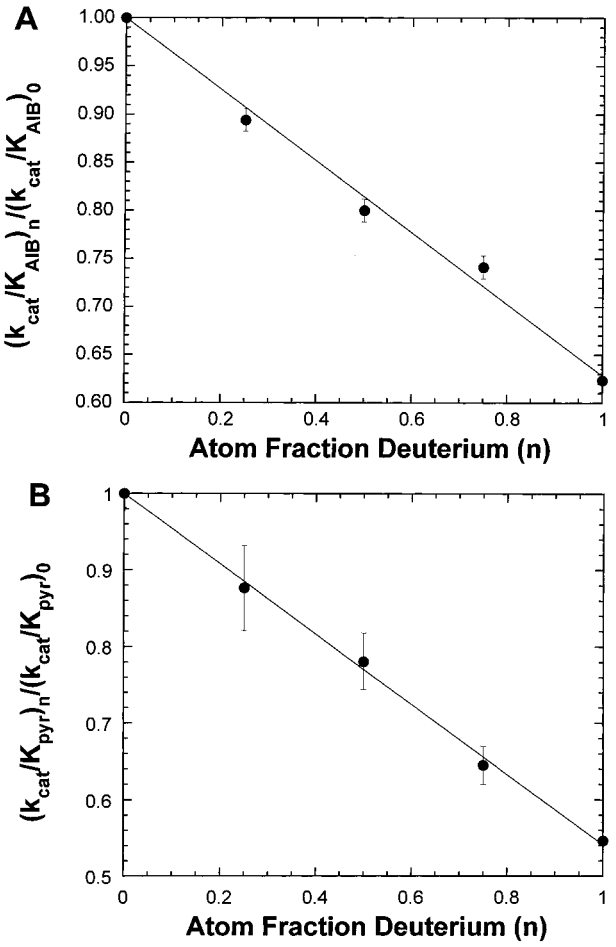

FIGURE 6: Proton inventories for the DGD catalyzed reaction between AIB and pyruvate. Reaction conditions: 30 mM bicine-KOH, pH 8.2, 50 mM dipotassium succinate, 0.5 unit/mL 2°ADH, 0.2 mM NADPH. Saturation curves for AIB were performed with 1 mM pyruvate and saturation curves for pyruvate were performed with 2 mM AIB. The fitted lines are least squares linear fits.

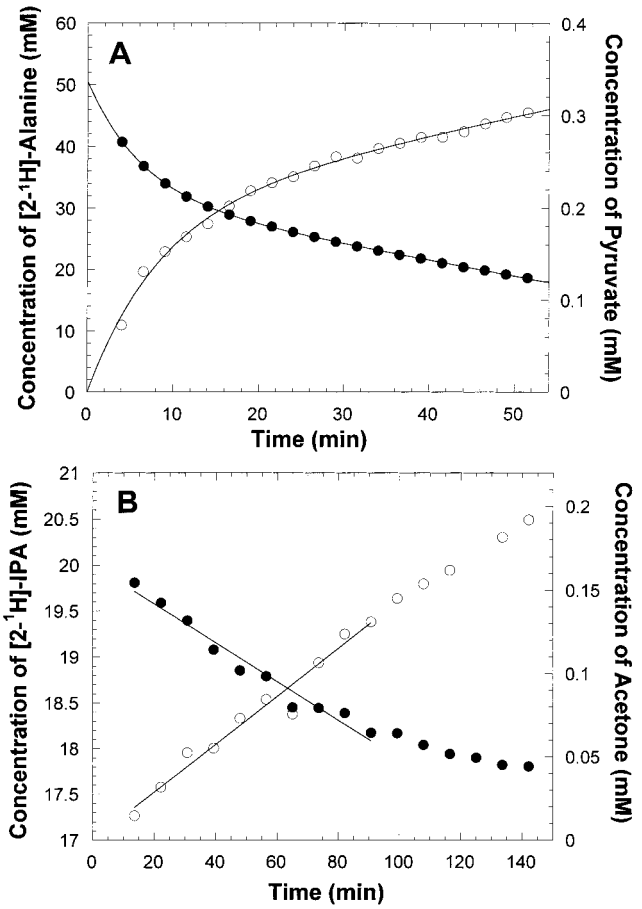

FIGURE 7: NMR determinations of washout vs product formation for the transamination of (A) L-alanine and (B) isopropylamine. The L-alanine data clearly indicate the conversion of the fast to the slow enzyme form and thus were fitted to eq 3, which describes a hysteretic enzyme. Linear fits for the isopropylamine data are shown and were used to calculate the ratio of washout to product formation.

The conclusion that protonation of the quinonoid intermediate on C4′ limits the L-alanine transamination half-reaction predicts, assuming the quinonoid intermediate can exchange the substrate derived proton with solvent, that the rate of exchange of the Cα hydrogen of L-alanine with solvent vs pyruvate formation should be fast. This number was measured in the NMR experiments to be 105 ± 30. The relatively large error notwithstanding, this shows definitively that quinonoid protonation is the rate-limiting step in the L-alanine/pyruvate transamination half-reaction, and defines the relative heights of the energy barriers facing the quinonoid intermediate. Thus, the protonation at C4′ to go forward to the ketimine intermediate is ∼2.8 kcal/mol higher in energy than is the reverse reaction to the external aldimine intermediate.

This analysis implies that reprotonation of the quinonoid intermediate at Cα should occur with a rate constant ∼100-fold greater than the k_{max} value observed in the L-alanine transamination half-reaction, or ∼2400 s^{-1}. The reverse reaction of DGD-PMP with pyruvate should thus show quinonoid absorbance rise and fall with rate constants of that for ketimine deprotonation at C4′ and ∼2400 s^{-1}. The values of the slow rate constant obtained from simple two-exponential fits to the 495 nm absorbance increase hyperbolically with pyruvate concentration to a maximal value of 75 s^{-1} (Figure 5). The concentration dependence and the agreement between the K_{app} values obtained from rate constants vs spectra, discussed above, demonstrates this step to be coupled to pyruvate association and is thus assigned to deprotonation of the ketimine at C4′. The fast phase rate constant, which would thus correspond to quinonoid reprotonation at Cα to give the L-alanine external aldimine intermediate, has a concentration independent value of ∼300 s^{-1}. This is substantially different from the expected value of ∼2400 s^{-1}.

The discrepancy between the rate constants apparently lies in the uncertainties in the enzyme concentration used in the experiment and the extinction coefficient of the quinonoid intermediate, as well as in the error on the ratio measured by NMR. The data in Figure 5 were also fitted using the mechanism of eq 2 and KINSIM/FITSIM with limited success for global analysis of all five data sets. What is clear from this exercise is that the fast-phase rate constant is highly correlated with the values of enzyme concentration and extinction coefficient. Thus, fast-phase values of >500 s^{-1} were obtained in fits where the extinction coefficient was assumed to be >20,000 M^{-1} cm^{-1}.

Concerted Decarboxylation/Proton Transfer in the AIB Half-Reaction. DGD shows extreme specificity in its catalysis of AIB decarboxylation; an undetectable amount of isopropylamine (less than 1 in 10^5 turnovers) is formed via

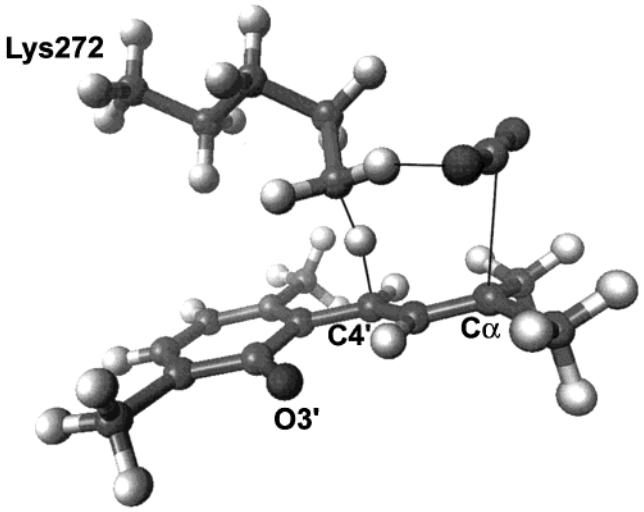

FIGURE 8: Hypothetical model for the proposed concerted decarboxylation/proton-transfer transition state for the AIB half-reaction. Partial bonds are indicated by the thin black lines. As shown, the ϵ-amino group of Lys272 is donating a proton to C4′ at the same time that the C$\alpha-CO_2^-$ bond is breaking. A hydrogen bond is shown between Lys272 and the departing CO_2.

replacement of the carboxylate group on Cα with a proton, while all detectable product is acetone, which arises from protonation at C4′. This specificity could be determined by enzyme−substrate interactions after formation of the quinonoid intermediate, or, as proposed below, by a concerted transition state in which the C4′-H and the C$\alpha-CO_2^-$ bonds are simultaneously being made and broken (Figure 8).

The pH studies (*7*) as well as the present data clearly demonstrate that AIB external aldimine formation is rapid and at equilibrium with respect to the rate-limiting step. The large (1.042 ± 0.009) [1-^{13}C]AIB KIE on the decarboxylation half-reaction indicates that this rate-limiting step involves substantial cleavage of the C$\alpha-CO_2^-$ bond, and is thus the decarboxylation step itself.

Absorbance for the quinonoid intermediate at 495 nm is not observed in the AIB decarboxylation half-reaction for any of the alkali metal ion forms of DGD-PLP. This could be due to either rapid reprotonation of the quinonoid, or to a concerted mechanism in which it is never formed. KINSIM simulations using the mechanism of eq 2, 25 mM AIB, 12 μM enzyme, 40 000 M^{-1} cm^{-1} for the quinonoid extinction coefficient, and 25 s^{-1} for the decarboxylation rate constant show that the rate constant for quinonoid protonation at C4′ would have to be >10 000 s^{-1} for no quinonoid absorbance to be detected in the stopped-flow traces. Although not impossible, this value is very large compared to that for the same chemical step in the L-alanine transamination half-reaction (25 s^{-1}).

The [4′-^{2}H]PLP KIE and the solvent KIE on k_{cat}/K_{AIB} also support a concerted decarboxylation/proton-transfer transition state. The inverse secondary KIE of 8% when [4′-^{2}H]PLP replaces PLP in the AIB decarboxylation half-reaction requires that C4′ undergoes substantial rehybridization from an sp^2 to an sp^3-like geometry in the transition state. No change in geometry at C4′, and thus no KIE, is expected in the decarboxylation step if the quinonoid intermediate, which is sp^2 hybridized at C4′, were formed. The solvent KIE of 1.5 on k_{cat}/K_{AIB} with a single proton in flight in the transition state (i.e., linear proton inventory) is consistent with a proton being transferred from Nϵ of Lys272 to C4′ in a concerted transition state, but this KIE is equivocal since other proton transfers (e.g., to or from the pyridine nitrogen) could account for it.

The final evidence presented here for a concerted decarboxylation/proton-transfer transition state is the value of 14 ± 1 for the relative rates of C2−H solvent exchange of isopropylamine vs product formation (acetone via transamination). The deprotonation of the external aldimine at C2 of isopropylamine yields a quinonoid intermediate with a chemical structure identical to that potentially obtained from AIB, assuming rapid CO_2 dissociation. If the mechanism for specificity of protonation at C4′ of PLP vs C2 of isopropylamine (or AIB) originates in enzyme−quinonoid interactions, then the identical quinonoid intermediates formed from isopropylamine or AIB should show identical protonation specificities. The washout-to-turnover ratio for isopropylamine is expected to be unity in this case, based on the observation that less than one in 10^5 turnovers of AIB occurs with protonation at Cα and the assumption that steps after ketimine formation are fast. This latter assumption is reasonable given the rapidity of pyruvate ketimine hydrolysis (*3*). The measured value of 14 ± 1 thus clearly indicates that enzyme−quinonoid interactions *are not* the determinant of C4′ vs C2 protonation specificity.

Combined, the [^{13}C]AIB KIE, the lack of detectable quinonoid absorbance, the secondary [^{2}H]PLP and solvent KIEs, and the large washout to product formation ratio strongly support a concerted transition state in which the C$\alpha-CO_2^-$ bond is being broken and the C4′−H bond is being made simultaneously. This transition state is likely not to be synchronous (i.e., equal bond breaking/bond making), rather C$\alpha-CO_2^-$ bond scission likely leads the process giving it substantial carbanionic character which could be stabilized as in other PLP reactions by the conjugated π system. Definitive proof of a concerted transition state awaits the measurement of multiple KIEs, both [^{13}C]AIB and [^{2}H]-PLP and [^{13}C]AIB and D_2O. [The observation of substantial amounts of nonoxidative decarboxylation with several alternative substrates (*8*) suggests that these suboptimal reactions do not follow the same concerted mechanism.]

Half-Reaction Free-Energy Profiles. The half-reaction kinetic parameters reported here should account well for the steady-state kinetic measurements, if the above interpretations of the kinetic and spectral data are correct. The simplified reaction sequence of Scheme 2 can be employed, given the above discussion. The values of the steady-state kinetic parameters in terms of the rate and equilibrium constants in Scheme 2 are as follows.

$$k_{cat} = \frac{k_2 k_5}{k_2 + k_5} \tag{4}$$

$$K_{AIB} = K_1 \frac{k_5}{(k_2 + k_5)} \tag{5}$$

$$K_{pyr} = K_4 \frac{k_2}{(k_2 + k_5)} \tag{6}$$

The calculated k_{cat} is 18.5 s^{-1}. Taking account that only 69% of the total enzyme is in the fast form (*3*), this value is reduced to 13.9 s^{-1}, in good agreement with the measured

Scheme 2

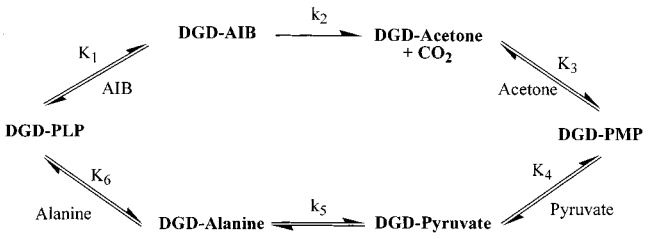

value of 13.1 ± 0.1 s^{-1}. The calculated value of K_{AIB} is 1.7 mM while that for K_{pyr} is 0.17 mM, in good agreement with the measured values of 1.6 ± 0.2 mM and 0.15 ± 0.03 mM, respectively (*7*).

In terms of Scheme 2, the observed [^{13}C]KIE can be expressed as follows (*17*).

$$^{13}k_{cat} = \frac{^{12}k_2/^{13}k_2 + R_f/E_f}{1 + R_f/E_f} \quad (7)$$

Here $E_f = 1$ and $R_f = k_2/k_5$. Assuming the intrinsic KIE to be 1.06 (*18*) and that the measured half-reaction KIE of 1.04 ± 0.01 is in agreement with this, the observed [^{13}C]KIE is calculated to be 1.045. This agrees with the measured value of 1.043 ± 0.003.

The half-reaction kinetic parameters thus validated, one can employ them in the construction of half-reaction free energy profiles. Figure 9 presents these. The profile for the AIB decarboxylation half-reaction (Figure 9A) shows the direct conversion of the external aldimine to the ketimine intermediate via a concerted transition state. This is the only kinetically significant transition state, the formation of the AIB external aldimine and hydrolysis of the acetone ketimine being very rapid in comparison. The relative energies of the Michaelis complexes were set by the values of K_{AIB} and K_i^{pyr} (10 mM; ref *7*). The former reflects contributions from both the Michaelis complex and external aldimine and the latter only the Michaelis complex (or rather the dead-end pyruvate complex, which is assumed to be indicative of the Michaelis complex). Decarboxylation is assumed to be irreversible, thus the relative energies of the external aldimine and ketimine, are undetermined. The lower energy of DGD-PMP and free acetone compared to the ketimine is based on the lack of significant inhibition of the AIB/pyruvate reaction at relatively low acetone concentrations (<200 mM).

The L-alanine half-reaction is somewhat more complicated (Figure 9B). The relative energies of the free enzyme, Michaelis complex, and external aldimine were set based on the values of K_{Ala} and K_i^{pyr}. The data in the inset to Figure 3B, showing that the quinonoid absorbance of species A rises to 0.003 with saturating L-alanine and 13 μM DGD-PLP, provides the energetic difference between the external aldimine and quinonoid intermediates based on a quinonoid extinction coefficient of 35 000 M^{-1} cm^{-1}. Protonation of the quinonoid intermediate is the rate determining step in the L-alanine to pyruvate direction and this barrier height is calculated from the k_{max} value for the L-alanine half-reaction. The value of ~100 for the washout vs product formation ratio determines the relative barrier heights for quinonoid protonation at Cα vs C4′ to give the external aldimine or ketimine, respectively. The barrier height for ketimine deprotonation at C4′, and thus the energetic difference between the quinonoid and ketimine, is obtained from the k_{max} value for the DGD-PMP reaction with pyruvate. Finally, the position of DGD-PMP and free pyruvate is determined either by the K_{pyr} value or the half-reaction equilibrium constant calculated from k_{max}/K for the forward and reverse half-reactions.

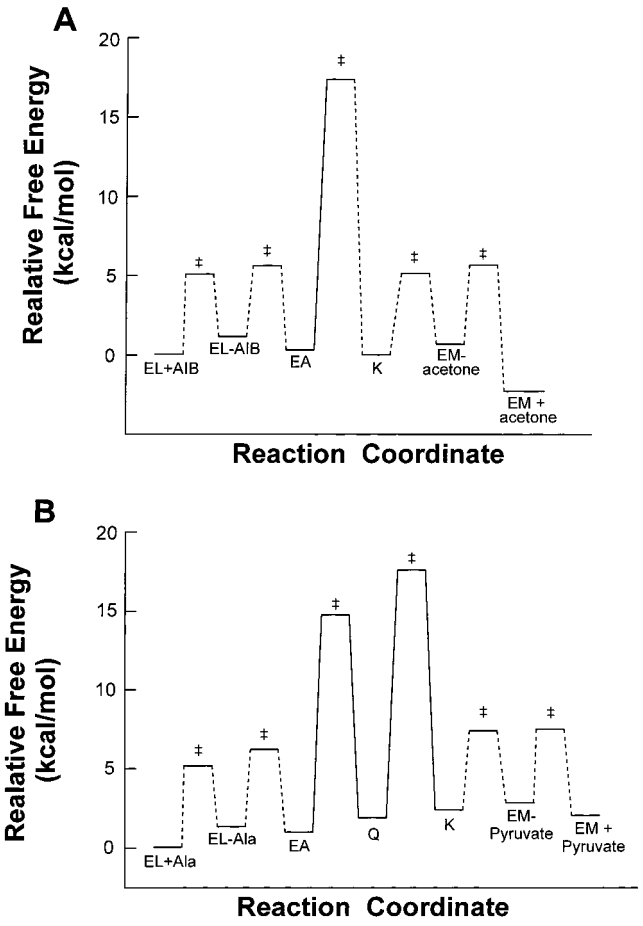

FIGURE 9: Free-energy profiles for the (A) AIB and (B) L-alanine/pyruvate half-reactions. The dashed lines indicate undetermined values for rate constants. The abbreviations are as follows: EL, DGD-PLP; EA, external aldimine; K, ketimine; EM, DGD-PMP.

Evolutionarily, DGD is an aminotransferase that has gained the ability to catalyze decarboxylation (*1*). These half-reaction energy profiles paint a picture of an aminotransferase that has compromised its transamination prowess for the sake of adapting to the needs of the rate-limiting Cα−CO_2^- cleavage step. The rate constant for Cα deprotonation of the L-alanine external aldimine is calculated from the free energy profile to be ~2000 s^{-1}. This is faster than even aspartate aminotransferase (*19*), a highly developed enzyme catalyzing only transamination. A major component of the adaptive restrictions placed on the enzyme by the decarboxylation half-reaction may well be the requirement for a concerted transition state to ensure specific protonation at C4′, with ensuing transfer of the substrate amino group to the coenzyme.

REFERENCES

1. Keller, J. W., Baurick, K. B., Rutt, G. C., O'Malley, M. V., Sonafrank, N. L., Reynolds, R. A., Ebbesson, L. O. E., and Vajdos, F. F. (1990) *J. Biol. Chem. 265*, 5531−5539.
2. Brueckner, H., and Przybylski, M. (1984) *J. Chromatogr. 296*, 263−275.

3. Zhou, X., Kay, S., and Toney, M. D. (1998) *Biochemistry 37*, 5761−5769.
4. Toney, M. D., Hohenester, E., Cowan, S. W., and Jansonius, J. N. (1993) *Science 261*, 756−759.
5. Toney, M. D., Hohenester, E., Keller, J. W., and Jansonius, J. (1995) *J. Mol. Biol. 245*, 151−179.
6. Hohenester, E., Keller, J. W., and Jansonius, J. N. (1994) *Biochemistry 33*, 13561−13570.
7. Zhou, X., and Toney, M. D. (1999) *Biochemistry 38*, 311−320.
8. Sun, S., Zabinsky, R., and Toney, M. D. (1998) *Biochemistry 37*, 3865−3875.
9. Sun, S., Bagdassarian, C. K., and Toney, M. D. (1998) *Biochemistry 37*, 3876−3885.
10. Julin, D. A., and Kirsch, J. F. (1989) *Biochemistry 28*, 3825−3833.
11. Goldberg, J. M., and Kirsch, J. F. (1996) *Biochemistry 35*, 5280−5291.
12. Phillips, R. S., Sundararaju, B., and Faleev, N. G. (2000) *J. Am. Chem. Soc. 122*, 1008−1014.
13. Florentiev, V. L.; Ivanov, V. I. and Karpeisky, M. Ya. (1968) *Methods Enzymol. 18A*, 567−581.
14. Kallen, R. G., Korpela, T., Martell, A. E., Matsushima, Y., Metzler, C. M., Metzler, D. E., Morozov, Y. V., Ralston, I. M., Savin, F. A., Torchinsky, Y. M., and Ueno, H. (1984) in *Transaminases* (Christen, P., and Metzler, D. E., Eds) John Wiley & Sons, New York.
15. Zhou, X., and Toney, M. D. (1998) *J. Am. Chem. Soc. 120*, 13282−13283.
16. Metzler, C. M., Harris, A. G., and Metzler, D. E. (1988) *Biochemistry 27*, 4923−4933.
17. Northrop, D. B. (1981) *Biochemistry 20*, 4056−4061.
18. Dunn, G. E. (1977) in *Isotopes in Organic Chemistry* (Buncel, E., and Lee, C. C., Eds.) Vol. 3, p 1, Elsevier, Amsterdam.
19. Hayashi, H., and Kagamiyama, H. (1997) *Biochemistry 36*, 13558−13569.

BI001237A